Rare Metal Materials and Engineering
Volume 52, Issue 5, May 2023
Available online at www.rmme.ac.cn

Science Press

Cite this article as: Li Junwei, Jia Weimin, Lv Shasha, et al. First-Principles Study of Surface Adsorption and Dissociation Behavior of O_2 on Uranium-Molybdenum System[J]. Rare Metal Materials and Engineering, 2023, 52(05): 1650-1660.

ARTICLE

First-Principles Study of Surface Adsorption and Dissociation Behavior of O_2 on Uranium-Molybdenum System

Li Junwei[1,2], Jia Weimin[2], Lv Shasha[3], Wang Jintao[2], Li Zhengcao[1]

[1] School of Materials Science and Engineering, Tsinghua University, Beijing 100084, China; [2] Xi'an Research Institute of High-Technology, Xi'an 710025, China; [3] College of Nuclear Science and Technology, Beijing Normal University, Beijing 100875, China

Abstract: The adsorption and dissociation behavior of O_2 molecules on U-Mo alloy surface was studied based on the first-principles simulation. One U atom at the highly symmetrical adsorption sites of the top layer was replaced by one Mo atom, and four U atoms at the top layer were replaced by four Mo atoms, resulting in the fact that γ-U(100)/Mo and γ-U(100)/4Mo slabs were established on the basis of the γ-U(100) slab with five layers. The configuration parameters, adsorption energy, Bader charge, electronic structure, and surface work function were calculated under different adsorption configurations. Results show that the O_2 molecules are chemically absorbed on the γ-U(100)/Mo and γ-U(100)/4Mo surfaces with the adsorption energy of −12.552 and −8.661 eV, respectively. The most stable adsorption configuration is the hollow horizontal adsorption configuration. The O_2 molecule adsorption on U-Mo alloy surface can be divided into dissociated adsorption and undissociated adsorption, which jointly contribute to the stable adsorption behavior. In addition, the dissociated adsorption is more stable than the undissociated adsorption. The Bader charge results show that during the oxygen adsorption, the charge transfer mainly occurs at the atoms of the top two layers of adsorption surface. The electronic structure results show that the slight overlapping hybridization occurs in O 2s with U 6p orbitals. Meanwhile, the strong overlapping hybridization occurs in O 2p with U 6d, Mo 5s, Mo 4p, and Mo 4d orbitals. This research clarifies the O_2 molecule adsorption mechanism on U-Mo alloy surface and provides theoretical basis for the oxidation corrosion mechanism of U-Mo alloy surface.

Key words: U-Mo alloy; dissociated adsorption; orbital hybridization; first-principles study

Uranium (U), one of the most complex actinide radiochemical elements, is the most important nuclear fuel in nuclear reactors in the nuclear industry. Depleted uranium produced by the enrichment process is usually used in the manufacture of tank armor and armor-piercing ammunition[1–3]. The complex electronic structure and strong correlation of 5f electrons[4] of U atoms result in its specific physical and chemical properties. Uranium is very susceptible to the surface corrosion by oxygen, hydrogen, and water at room temperature[5–8]. The uranium metal can be oxidized rapidly to form a compact oxide layer once it is exposed to oxygen. A certain amount of alloying elements (Mo, Nb, Zr, Ti, and Hf) can be added into U to improve the corrosion resistance[9–12] and machinability.

Among the uranium alloys, U-Mo alloy attracts much attention[12]. The oxidation corrosion of U-Mo alloy mainly contains the adsorption and dissociation of O_2 molecules. However, the experimental investigation of uranium[13–14] can hardly be conducted. Therefore, the theoretical calculation is proposed and used to study the adsorption and dissociation behavior of O_2 molecules on U-Mo alloy surface.

The first-principles method has been widely used to study the adsorption and dissociation of O_2 molecules on uranium and uranium alloys. Huda et al[15] studied the O_2 adsorption on (100) surface of γ-uranium by density functional study. It is found that the O 2p orbital hybridizes with U 5f band, and some U 5f electrons become more localized in the adsorption process. Liu et al[16] studied the adsorption and diffusion properties of oxygen atoms on the (100) surface of α-U material by the first-principles method, and reported that the

Received date: June 19, 2022
Foundation item: National Natural Science Foundation of China (11975135, 12005017); National Basic Research Program of China (2020YFB1901800)
Corresponding author: Li Zhengcao, Ph. D., Professor, School of Materials Science and Engineering, Tsinghua University, Beijing 100084, P. R. China, Tel: 0086-10-62772233, E-mail: zcli@tsinghua.edu.cn

low diffusion barrier of the O atom results in the formation of uranium-oxide layer on the surface. Besides, the diffusion barrier of the O atom is high from the surface to the sub-surface. Thus, the O atom cannot migrate to the sub-surface easily. Liu et al[17] studied the adsorption of O atoms on the Ti-doped γ-U (001) surface and found that Ti-doping can reduce the diffusion of O atoms. Tian et al[18] calculated the adsorption of O atoms on the γ-U(110) surface and investigated the Mo doping effect on the γ-U(110) surface. The short bridge site is the most stable adsorption site for O atom on the γ-U(110) surface. The doped Mo atom reduces the adsorption energy of O atom at all adsorption sites and increases the energy barrier of O atom diffusion.

To further explore the influence of Mo doping on the oxidation corrosion of U-Mo alloy, the adsorption and dissociation behavior of O_2 molecules on γ-U(100)/Mo and γ-U(100)/4Mo surface was investigated by the first-principles calculation in this research. The γ-U(100) surface is more symmetrical than the γ-U(110) surface, and the surface energy of (100) crystal face is larger than that of (110) crystal face, which leads to the adsorption and easy corrosion. Thus, the γ-U(100) surface was selected for calculation. The formation energy of a single vacancy is 1.054 eV, which agrees well with the results in Ref.[19] (1.08 eV). The formation energy of Mo substitution, Mo interstitial at tetrahedral site, and Mo interstitial at octahedral site is 0.175, 1.028, and 2.873 eV, respectively. It can be seen that the doped Mo atoms thermodynamically prefer to substitute U atoms in γ-U configuration rather than tetrahedral or octahedral vacancies. Thus, two types of γ-U(100) slabs of 5 layers were established. One U atom at the highly symmetrical adsorption sites of the top layer was replaced by one Mo atom, and four U atoms at the top layer were replaced by four Mo atoms, which correspond to the adsorption site models of O_2 molecules on γ-U(100)/Mo and γ-U(100)/4Mo, respectively. The relaxations of adsorption configurations were conducted. The adsorption configurations, adsorption energy, Bader charge, surface work function, and electronic structure were investigated.

1 Numerical Simulation and Model Establishment

1.1 Numerical method

The Vienna Ab-initio simulation package (VASP 5.4.4) was used for calculations[20–21] based on the density functional theory (DFT)[22–23] in this research, which could accurately and efficiently expand the crystal wave function. The electron-ion interaction was studied by the projected augmented wave pseudopotential method, which is widely used to calculate the electronic structure in the surface atoms[24]. Perdew-Burke-Ernzerhof (PBE) exchange correlation potential approximation in generalized gradient approximation (GGA) was used to calculate the electron exchange correlation[25–26]. The GGA-PBE pseudopotentials were used for U, Mo, and O atoms. The U atom had 14 valence electrons ($6s^26p^67s^25f^36d^1$), and the Mo atom had 12 valence electrons ($4p^64d^55s^1$). The O atom had 6 valence electrons ($2s^22p^4$) in the outer layer. The Methfessel-Paxton method was applied to calculate the configuration of extra-nuclear electron orbitals. In Brillouin zone, the Monkhorst-Pack method was used to automatically obtain irreducible k-point[27]. The k-point grid parameters of the surface model and adsorption configurations were set as 5×5×1, and those for the density of states were set as 7×7×1. In self-consistent cycle calculation, the energy difference between adjacent iterations was less than 1×10^{-6} eV to satisfy the energy convergence criterion. The force convergence criterion in geometric optimization was that the residual force should be less than 0.1 eV/nm. Conjugate gradient method[28] was applied to obtain the configuration of the lowest energy after structure optimization. The cut-off energy of plane wave was 500 eV, and the spin polarization was neglected in all optimization calculations[29].

The adsorption energy (E_{ads}) can be defined as follows:

$$E_{ads} = E_{slab+B} - E_{slab} - E_B \quad (1)$$

where E_{slab+B} is the total energy of the slab after adsorption of oxygen molecule, E_{slab} is the total energy of the slab, and E_B represents the energy of the oxygen molecule. The energies before and after adsorption could both be calculated by Eq.(1). When the system is stable after O_2 adsorption, the adsorption energy is negative and the system energy is the lower before the adsorption state. On the contrary, the positive adsorption energy indicates the system is unstable after adsorption.

1.2 Numerical model

γ-U cell has body-centered cubic structure with space group symbol of Im3m, and its lattice constants *a*, *b*, and *c* are 0.3532 nm[30]. The lattice constant was optimized as 0.3433 nm in this research, and the difference between calculated and theoretical values was 2.803%. The O_2 molecule has linear structure, and the bond length of the O atom is 0.1208 nm[31]. The O_2 molecule was packed in a box with side length of 1 nm, and the bond length of O atom was 0.1234 nm. The difference between the calculated and theoretical values was 2.152%.

The U atomic surface model of five layers (*p*-U model, 2×2) was established to simulate the γ-U(100) surface based on the lattice constants of the γ-U cell after optimization. The three layers at bottom were fixed, and the top two layers of the slab model were free to relax. The structure optimization for γ-U(100)/Mo and γ-U(100)/4Mo slabs was conducted. In order to reduce the interactions between the adjacent layers, a vacancy with length of 1.5 nm was set on the *z*-axis of these two structures[32]. The surface model was modified along *z*-axis to eliminate the non-zero dipole caused by the asymmetry of the surface model[33]. Fig.1 shows the schematic diagrams of the γ-U(100)/Mo and γ-U(100)/4Mo slabs after structure optimization.

The highly symmetrical adsorption sites for O_2 molecule included the top, bridge, and hollow sites, and the adsorption modes could be divided into two types: (1) the O_2 molecule was horizontal to the γ-U(100)/Mo and γ-U(100)/4Mo surfaces (Hor type); (2) the O_2 molecule was vertical to γ-U(100)/Mo and γ-U(100)/4Mo surfaces (Ver type).

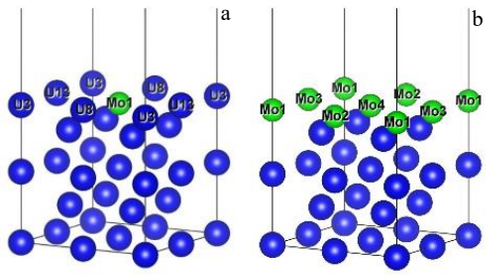

Fig.1 Schematic diagrams of γ-U(100)/Mo (a) and γ-U(100)/4Mo (b) slabs after structure optimization

The O_2 adsorption of the γ-U(100)/Mo slab model included 19 U atoms, 1 Mo atom, and 1 O_2 molecule. The adsorption configurations included 6 types: top-horizontal (T-Hor) type, top-vertical (T-Ver) type, hollow-horizontal (H-Hor) type, hollow-vertical (H-Ver) type, bridge-horizontal (B-Hor) type, and bridge-vertical (B-Ver) type. Fig.2 shows the top and side views of adsorption models of O_2 molecule on the γ-U(100)/Mo surface.

The O_2 adsorption of the γ-U(100)/4Mo slab model included 16 U atoms, 4 Mo atoms, and 1 O_2 molecule. To distinguish the O_2 adsorption of the γ-U(100)/Mo slab model from that of the γ-U(100)/4Mo slab model, six adsorption configurations were established: 4-top-horizontal (4-T-Hor) type, 4-top-vertical (4-T-Ver) type, 4-hollow-horizontal (4-H-Hor) type, 4-hollow-vertical (4-H-Ver) type, 4-bridge-horizontal (4-B-Hor) type, and 4-bridge-vertical (4-B-Ver) type. Meanwhile, the monolayer adsorption coverage (θ) of O_2 is 0.25 ML. Fig.3 shows the top and side views of adsorption models of O_2 molecule on the γ-U(100)/4Mo surface.

2 Results and Discussion

2.1 Configuration of adsorption and adsorption energy

Six types of highly symmetrical sites of O_2 adsorption for the γ-U(100)/Mo and γ-U(100)/4Mo slab models are optimized. After simplification, the top horizontal sites of γ-U(100)/Mo and γ-U(100)/4Mo slabs during O_2 adsorption are regarded as T-Hor and 4-T-Hor sites, respectively. The top

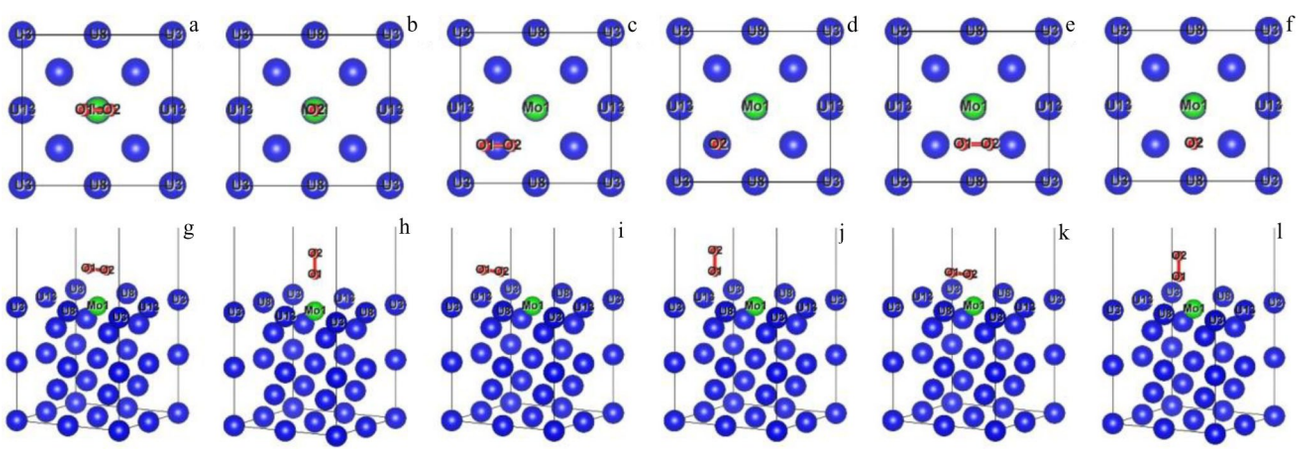

Fig.2 Top (a–f) and side (g–l) views of adsorption models of O_2 molecule on γ-U(100)/Mo surface: (a, g) T-Hor type, (b, h) T-Ver type, (c, i) H-Hor type, (d, j) H-Ver type, (e, k) B-Hor type, and (f, l) B-Ver type

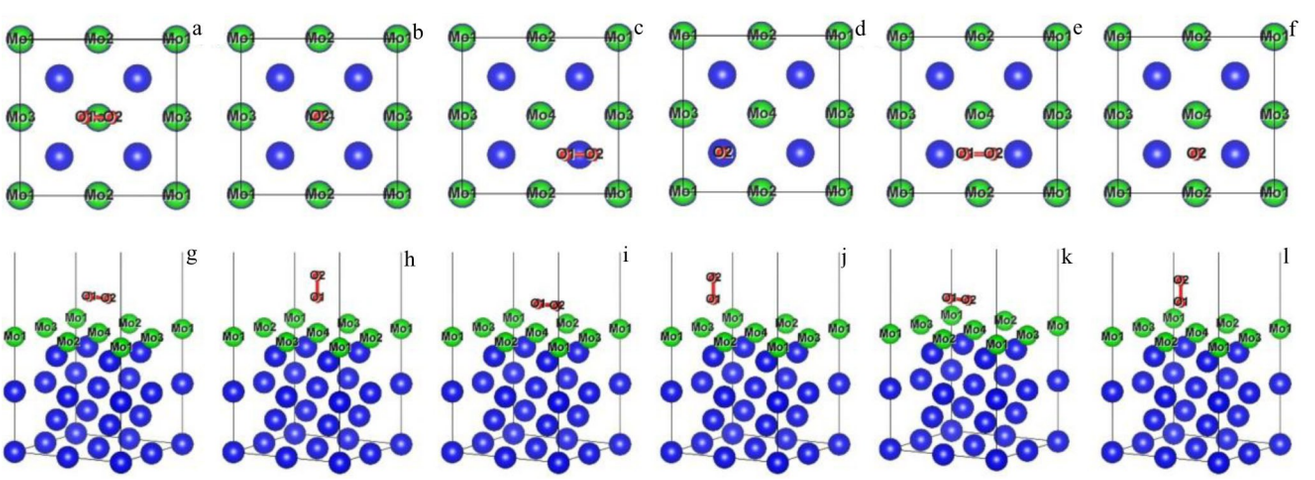

Fig.3 Top (a–f) and side (g–l) views of adsorption models of O_2 molecule on γ-U(100)/4Mo surface: (a, g) 4-T-Hor type, (b, h) 4-T-Ver type, (c, i) 4-H-Hor type, (d, j) 4-H-Ver type, (e, k) 4-B-Hor type, and (f, l) 4-B-Ver type

and side views of adsorption models of O_2 molecule on γ-U(100)/Mo slab surface after structure relaxation are shown in Fig.4, and those on γ-U(100)/4Mo slab surface after structure relaxation are shown in Fig.5. Table 1 and Table 2 show the adsorption energy and related geometrical parameters of O_2 adsorption on γ-U(100)/Mo and γ-U(100)/4Mo slab surfaces, respectively.

According to Fig.4 and Table 1, the surface atoms of the top two layers are relaxed significantly when the O_2 molecule is absorbed on the γ-U(100)/Mo slab surface. The distance between O1 and O2 atoms ($d_{O1\text{-}O2}$=0.2503–0.4290 nm) increases greatly, compared with the bond length of the O atom (0.1234 nm), except for the distance in configuration of T-Ver type. Currently, the O-O bond breaks, and the O_2 molecule is completely dissociated into two O atoms absorbed on the γ-U(100)/Mo slab surface. Among these five configurations, O atoms are approximately located at bridge and hollow positions after structure optimization. The $d_{O1\text{-}O2}$ is 0.1302 nm in the T-Ver configuration, indicating that the O_2 is adsorbed on the surface without dissociation.

According to Fig. 5 and Table 2, for the O_2 adsorption of γ-U(100)/4Mo slab surface, the $d_{O1\text{-}O2}$ in 4-H-Hor and 4-B-Hor configurations is 0.3670 and 0.2490 nm, respectively. The O_2 molecule is dissociated into two O atoms, and they are absorbed on the slab surface. In the 4-H-Hor and 4-B-Hor configurations, O atoms prefer to occupy the bridge and hollow positions, respectively. Meanwhile, for 4-T-Hor, 4-T-Ver, 4-H-Ver, and 4-B-Ver configurations, the O_2 molecule is adsorbed on surface without dissociation.

Fig. 6 shows the O_2 adsorption energy of γ-U(100)/Mo and γ-U(100)/4Mo surfaces. According to Fig.6 and Table 1, the energy of O_2 adsorbed on γ-U(100)/Mo surface is from −12.152 eV to −2.575 eV. The O_2 adsorption energy of the H-Hor configuration is the lowest of −12.152 eV, indicating the most stable adsorption structure of γ-U(100)/Mo slab. In addition, the adsorption energy of O_2 on γ-U(100)/4Mo is from −8.551 eV to −1.904 eV. The 4-H-Hor configuration has the lowest adsorption energy of –8.551 eV, indicating the most stable adsorption configuration of γ-U(100)/4Mo slab. The H-Hor configuration has the most stable sites because of its

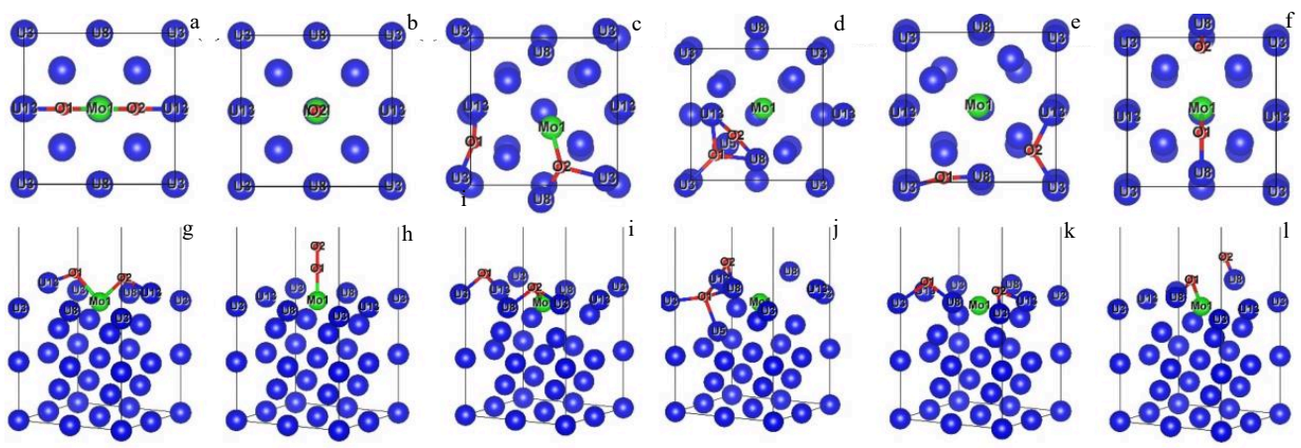

Fig.4 Top (a–f) and side (g–l) views of adsorption models of O_2 molecule on γ-U(100)/Mo surface after structure relaxation: (a, g) T-Hor type, (b, h) T-Ver type, (c, i) H-Hor type, (d, j) H-Ver type, (e, k) B-Hor type, and (f, l) B-Ver type

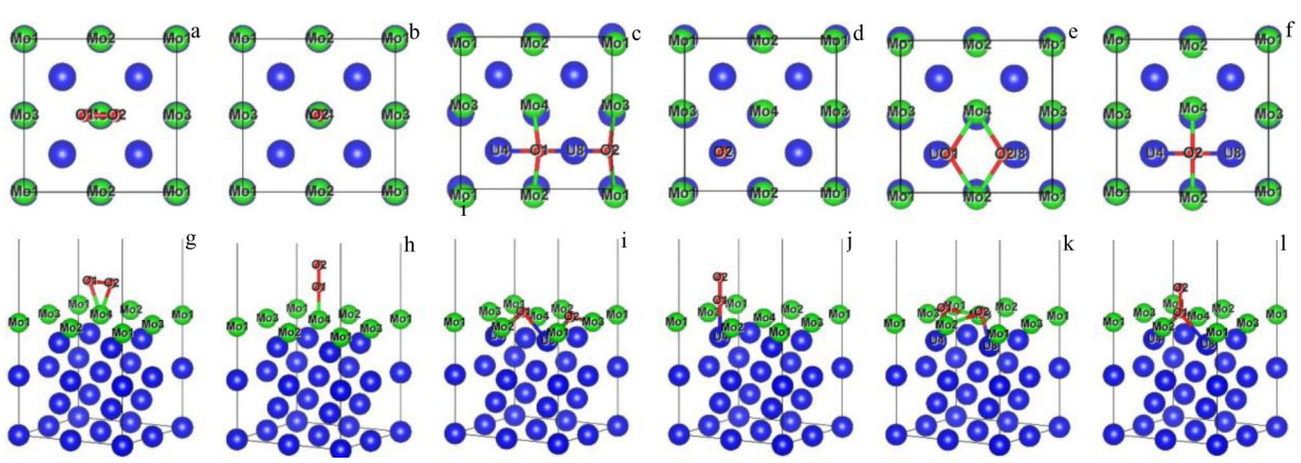

Fig.5 Top (a–f) and side (g–l) views of adsorption models of O_2 molecule on γ-U(100)/4Mo surface after structure relaxation: (a, g) 4-T-Hor type, (b, h) 4-T-Ver type, (c, i) 4-H-Hor type, (d, j) 4-H-Ver type, (e, k) 4-B-Hor type, and (f, l) 4-B-Ver type

Table 1 Adsorption energy and related geometrical parameters of O_2 adsorption on the first layer of γ-U(100)/Mo surface

Configuration	Adsorption energy, E_{ads}/eV	Distance between O1 and O2 atoms, $d_{O1\text{-}O2}$/nm	O1 atom bonding type, B_1	Bond length between O1 atom and surface atom, d_{B1}/nm	Optimal distance between O1 atom and surface atom, $h_{O1\text{-}S}$/nm	O2 atom bonding type, B_2	Bond length between O2 atom and surface atom, d_{B2}/nm	Optimal distance between O2 atom and surface atom, $h_{O2\text{-}S}$/nm
T-Hor	−9.001	0.3270	O1-U13	0.1938	0.1373	O2-U13	0.1938	0.1373
			O1-Mo	0.2240	-	O2-Mo	0.2240	-
T-Ver	−2.575	0.1302	O1-Mo	0.1868	0.1935	-	-	0.3237
H-Hor	−12.152	0.4252	O1-U3	0.2097	0.1289	O2-U3	0.2277	0.0987
			O1-U13	0.2064		O2-U8	0.2081	-
						O2-Mo	0.2267	-
H-Ver	−9.974	0.2503	O1-U3	0.2220	−0.0211			
			O1-U5	0.2298	-	O2-U8	0.2125	0.1849
			O1-U8	0.2261	-			
			O1-U13	0.2261	-	O2-U13	0.2125	-
B-Hor	−12.054	0.4290	O1-U3	0.2230	0.1321	O2-U3	0.2222	0.0950
			O1-U8	0.1999	-	O2-U13	0.2106	-
B-Ver	−9.608	0.4016	O1-U8	0.1995	0.1407	O2-U8	0.1835	0.2159
			O1-Mo	0.2061	-	-	-	-

Table 2 Adsorption energy and related geometrical parameters of O_2 adsorption on γ-U(100)/4Mo surface

Configuration	Adsorption energy, E_{ads}/eV	Distance between O1 and O2 atoms, $d_{O1\text{-}O2}$/nm	O1 atom bonding type, B_1	Bond length between O1 atom and surface atom, d_{B1}/nm	Optimal distance between O1 atom and surface atom, $h_{O1\text{-}S}$/nm	O2 atom bonding type, B_2	Bond length between O2 atom and surface atom, d_{B2}/nm	Optimal distance between O2 atom and surface atom, $h_{O2\text{-}S}$/nm
4-T-Hor	−2.681	0.1431	O1-Mo4	0.2009	0.2073	O2-Mo4	0.2009	0.2073
4-T-Ver	−2.825	0.1286	O1-Mo4	0.1876	0.2031	-	-	0.3317
4-H-Hor	−8.551	0.3670	O1-Mo2	0.2129	0.0589	O2-Mo1	0.2129	0.589
			O1-Mo4	0.2129	-	O2-Mo3	0.2129	-
			O1-U4	0.2395	-	O2-U4	0.2395	-
			O1-U8	0.2212	-	O2-U8	0.2212	-
4-H-Ver	−1.904	0.1345	O1-U4	0.2114	0.1132	-	-	0.2477
4-B-Hor	−6.912	0.2490	O1-Mo2	0.2370	0.0684	O2-Mo2	0.2370	0.0684
			O1-Mo4	0.2370	-	O2-Mo4	0.2370	-
			O1-U4	0.1993	-	O2-U8	0.1993	-
4-B-Ver	−2.825	0.1442	O1-Mo2	0.2083	0.0542	-	-	0.1983
			O1-Mo4	0.2083	-	-	-	
			O1-U4	0.2432	-	-	-	
			O1-U8	0.2432	-	-	-	

high symmetry on the γ-U(100)/Mo and γ-U(100)/4Mo surfaces after O_2 adsorption. For the O_2 adsorption energy of γ-U(100)/Mo and γ-U(100)/4Mo surfaces, the adsorption energy of all configurations is more than 40 kJ·mol^{-1}, indicating the chemical adsorption. The dissociation adsorption energy is significantly less than the undissociated adsorption energy, and the dissociated adsorption is more stable than the undissociated adsorption.

According to the bond lengths between O atoms and U/Mo atoms of γ-U(100)/Mo and γ-U(100)/4Mo surfaces, the distance between the O atom and the nearest U atom is 0.1938–0.2432 nm, which is close to the bond length of O-U in UO_2 (0.237 nm)[34]. This result indicates that a stable chemical bond forms between the O and U atoms on the surface. Similarly, the distance between the O atom and the nearest Mo atom is 0.1868–0.2370 nm, which is similar to the bond length of O-Mo in MoO_2 (0.198 nm)[35]. This result suggests that the stable chemical bond forms between O atom and Mo atom on

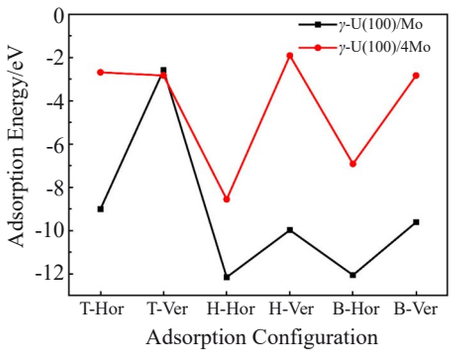

Fig.6 Adsorption energy of O_2 molecule on γ-U(100)/Mo and γ-U(100)/4Mo surfaces

the surface. In the H-Ver configuration, the optimal distance between O1 atom and surface atom $h_{O1\text{-}S}$ of −0.0211 nm shows that the O1 atom is located between the top first layer and the top second layer in the γ-U(100)/Mo slab. The O1 atom moves across the surface and diffuses into the γ-U(100)/Mo subsurface, forming a chemical bond (O1-U5) with the U atom of the second layer.

2.2 Bader charge distribution

The charge transfer between atoms reflects the interaction mechanism in the adsorption process. To clarify the adsorption mechanism of O_2 molecule, the Bader charge distribution results of O_2 adsorption on γ-U(100)/Mo and γ-U(100)/4Mo surfaces were calculated[36], as shown in Table 3. The negative net charge indicates that the system loses electrons and is positively charged, and the corresponding valence is positive. On the contrary, the positive net charge means the system gains electrons and is negatively charged.

The electronegativity of O, U, and Mo atoms is 3.44, 1.38, and 2.16[37], respectively. Since the electronegativity of the O atom is greater than that of U and Mo atoms on the surface, the charge transfers from U and Mo atoms to O atoms after adsorption. The total Bader charge number of the O_2 molecule is 0.7025–2.3671 e, indicating that O atoms form strong ionic bonds with the U and Mo atoms on the surface after the O_2 molecules adsorption on γ-U(100)/Mo slab surface. Similarly, the total Bader charge number of O_2 molecule is 0.5685 – 2.2138 e in O_2 molecule adsorption on γ-U(100)/4Mo slab surface. The Bader charge number of O_2 molecule of dissociated adsorption (1.9326 – 2.3671 e) is significantly larger than that of O_2 molecule of undissociated adsorption (0.5685–1.1961 e). This result indicates that the dissociated adsorption can form stronger and more stable ionic bonds than the undissociated adsorption does for O_2 adsorption on γ-U(100)/Mo and γ-U(100)/4Mo surfaces.

According to the total Bader charge number of the 1st–5th layers of γ-U(100)/Mo and γ-U(100)/4Mo surfaces, the Bader charge number mainly changes at the first and the second layers after O_2 adsorption. The O atoms mainly interact with the U and Mo atoms and the charge basically all transfers from U and Mo atoms to O atoms at the surface. Fig.7 shows the schematic diagrams of atom charge of the most stable adsorption configurations before and after O_2 molecule adsorption. The charge transfer from U/Mo atoms to O atoms leads to the positively charged U and Mo atoms and negatively charged O atoms after O_2 molecule adsorption.

Table 3 Bader charge distribution results of O_2 adsorption on γ-U(100)/Mo and γ-U(100)/4Mo surfaces (e)

Configuration	Bader charge number of O1 atom, q_{O1}	Bader charge number of O2 atom, q_{O2}	Total Bader charge number of O1 and O2 atoms, q_{total}	q_{1st}	q_{2nd}	q_{3rd}	q_{4th}	q_{5th}
Atom	0.1452	−0.1452	0	-	-	-	-	-
γ-U(100)/Mo	-	-	-	−0.0931	0.2681	−0.4432	0.8123	−0.5880
T-Hor	1.0265	1.0265	2.0530	−1.8846	−0.1124	−0.2723	0.7302	−0.5549
T-Ver	0.5095	0.1930	0.7025	−0.8647	0.2774	−0.3339	0.7579	−0.5835
H-Hor	1.1292	1.1304	2.2596	−2.4400	0.2783	−0.3343	0.8303	−0.6355
H-Ver	1.2393	1.1278	2.3671	−2.3289	0.0198	−0.3383	0.8367	−0.6004
B-Hor	1.1231	1.1675	2.2906	−2.2606	0.0587	−0.3515	0.8764	−0.6558
B-Ver	1.0153	0.9173	1.9326	−2.0351	0.1076	−0.2110	0.8017	−0.6357
γ-U(100)/4Mo	-	-	-	1.0060	−0.6764	−0.6701	0.8737	−0.5745
4-T-Hor	0.4976	0.3195	0.8171	0.1620	−0.6928	−0.5858	0.7875	−0.5278
4-T-Ver	0.4724	0.0961	0.5685	0.4270	−0.7055	−0.6184	0.7853	−0.5281
4-H-Hor	1.1069	1.1069	2.2138	−0.1418	−1.7588	−0.7302	0.9631	−0.5861
4-H-Ver	0.6288	0.3217	0.9505	0.3006	−0.8507	−0.7837	0.9436	−0.6014
4-B-Hor	1.0072	1.0247	2.0319	−0.2011	−1.4721	−0.6938	0.8450	−0.5503
4-B-Ver	0.8387	0.3574	1.1961	0.2073	−1.1301	−0.6339	0.8805	−0.5601

Note: q_{1st}, q_{2nd}, q_{3rd}, q_{4th}, and q_{5th} are the total Bader charge number of the 1st, 2nd, 3rd, 4th, and 5th layers on γ-U(100)/Mo or γ-U(100)/4Mo surfaces, respectively

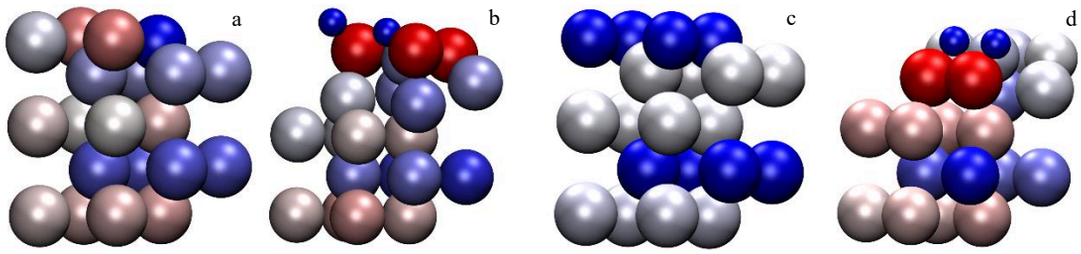

Fig.7 Schematic diagrams of atom charge of the most stable adsorption configurations before (a, c) and after (b, d) O_2 molecule adsorption: (a) γ-U(100)/Mo type, (b) H-Hor type, (c) γ-U(100)/4Mo type, and (d) 4-H-Hor type (red atoms are positively charged; blue atoms are negatively charged; the charge range is from −0.80 e to 0.80 e)

2.3 Electronic structure

2.3.1 Partial density of states

Fig.8 shows the partial density of states (PDOS) of O_2 molecule adsorption on γ-U(100)/Mo and γ-U(100)/4Mo surfaces of H-Hor and 4-H-Hor configurations, respectively. The Fermi energy (E_F) is also shown in Fig. 8. As shown in Fig. 8, the slight overlapping hybridization occurs between O 2s and U 6p orbitals from −25 eV to −15 eV in the H-Hor and 4-H-Hor configurations. The strong overlapping hybridization occurs in O 2p with U 6d, Mo 5s, Mo 4p, and Mo 4d orbitals in the vicinity energy of −5 eV, indicating that the O atoms cooperate with U and Mo atoms to form stable bonds after O_2 adsorption. The degree of overlapping hybridization of O and Mo atoms in the 4-H-Hor configuration is more serious than that of the H-Hor configuration, suggesting that the bonds between O and Mo atoms are more stable in the 4-H-Hor configuration.

2.3.2 Differential charge density

Fig.9 shows that differential charge density distributions for O_2 molecule adsorption on γ-U(100)/Mo and γ-U(100)/4Mo surfaces with H-Hor and 4-H-Hor configurations, respectively. The red atoms represent the atoms with increased charge density, and the yellow atoms represent the atoms with decreased charge density (isosurface level is 4 e/nm^3). After O_2 molecule adsorption, O atoms bond with U and Mo atoms near the slab surface, and the electrons gather around O atoms, resulting in the increase in the charge density. The U and Mo atoms lose electrons, leading to decreased charge density. The charge transfer mainly occurs at the top two layers of atoms, i. e., no apparent charge transfer occurs with the atoms of bottom three layers.

2.3.3 Total density of states

The total density of states (TDOS) of O_2 molecule before and after O_2 molecule adsorption are shown in Fig. 10. The highest occupied molecular orbital is $2\pi^*$ antibonding orbital before adsorption. All occupied orbitals of the O_2 molecule disappear after adsorption. At the energy from −25 eV to −15 eV, the 3σ and $4\sigma^*$ orbital overlapping are hybridized with the U 6p orbital. Meanwhile, the energy reduction of the $2\pi^*$ orbital occurs, which leads to the hybridization of $2\pi^*$ orbital with the 1π and 5σ orbitals. The 1π, 5σ, and $2\pi^*$ orbitals are hybridized with U 6d, Mo 5s, Mo 4p, and Mo 4d in the vicinity energy of −5 eV. Based on the overlapping hybridization, O atoms form new chemical bonds with the U and Mo atoms in the γ-U(100)/Mo and γ-U(100)/4Mo slab surfaces during the adsorption process. Briefly, the bonding mode between O and U/Mo atoms is dominated by ionic bonding, and the reaction mechanism is the weak hybridization of O 2s orbital with U 6p orbital coupled with the strong hybridization of O 2p orbital with U 6d, Mo 5s, Mo 4p, and Mo 4d orbitals.

2.4 Surface work function

The work function of γ-U(100)/Mo and γ-U(100)/4Mo slabs was analyzed before and after O_2 molecule adsorption. Work function refers to the minimum energy required for electrons

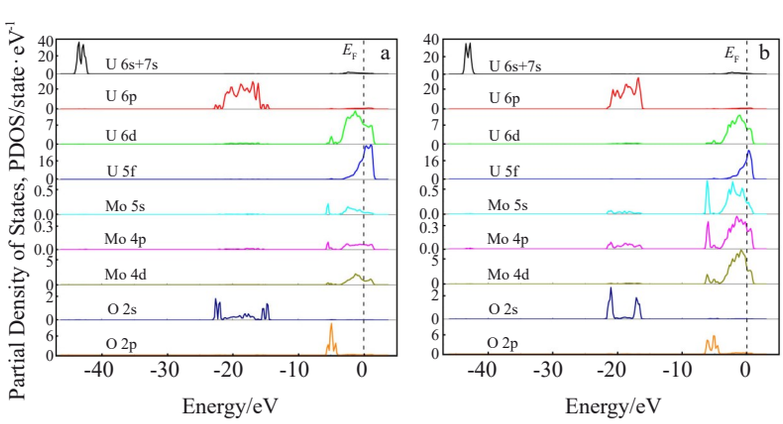

Fig. 8 PDOS of O_2 molecule adsorption on γ-U(100)/Mo surface with H-Hor configuration (a) and on γ-U(100)/4Mo surface with 4-H-Hor configuration (b)

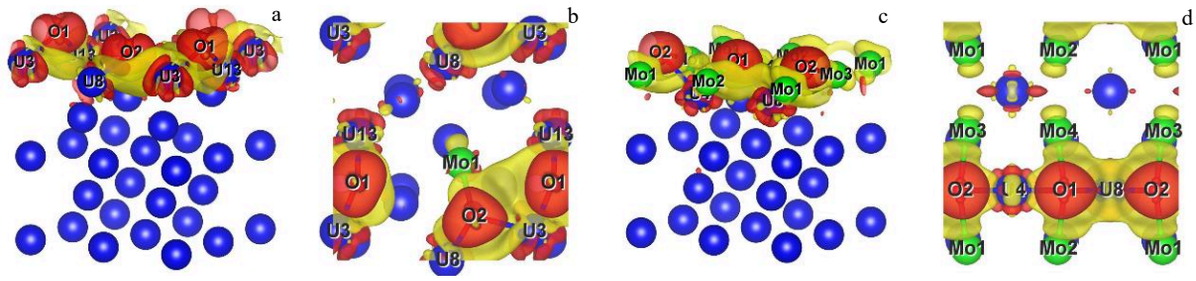

Fig.9 Side (a, c) and top (b, d) views of differential charge density distributions for O_2 molecule adsorption on γ-U(100)/Mo surface with the most stable H-Hor configuration (a–b) and on γ-U(100)/4Mo surface with the most stable 4-H-Hor configuration (c–d)

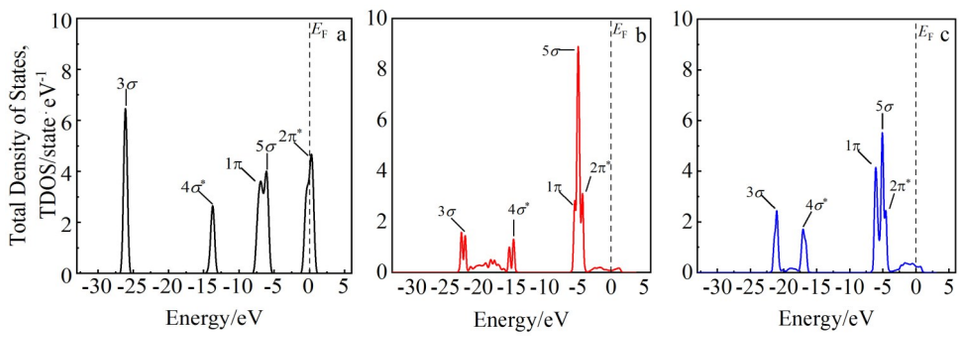

Fig.10 TDOS of O_2 molecule before adsorption (a); TDOS of O_2 molecule adsorption on γ-U(100)/Mo surface with the most stable H-Hor configuration (b) and on γ-U(100)/4Mo surface with the most stable 4-H-Hor configuration (c)

to move from the solid interior to the surface, which can be evaluated by the energy difference between the vacuum electrostatic potential at an infinite distance outside the metal and Fermi level, representing the ability of electrons to escape to the metal surface. Therefore, the work function can be expressed as follows:

$$\Phi = E_{vacuum} - E_{Fermi} \quad (2)$$

where Φ, E_{vacuum}, and E_{Fermi} represent the work function, vacuum level, and Fermi level, respectively. Fig.11 and Fig.12 show the distributions of electrostatic potential along the z-axis on the γ-U(100)/Mo and γ-U(100)/4Mo surfaces after O_2 molecule adsorption, and the corresponding surface work function changes are shown in Table 4 and Table 5, respectively.

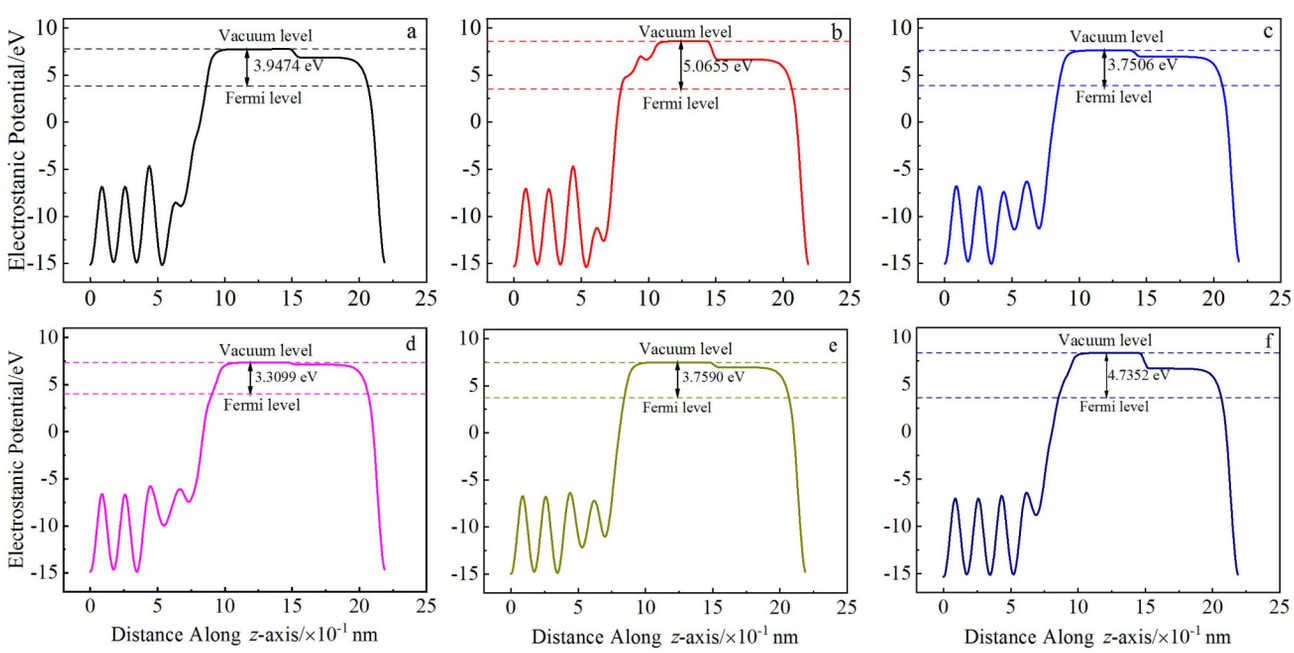

Fig.11 Electrostatic potential distributions along z-axis on γ-U(100)/Mo slab surfaces with different configurations after O_2 molecule adsorption: (a) T-Hor type, (b) T-Ver type, (c) H-Hor type, (d) H-Ver type, (e) B-Hor type, and (f) B-Ver type

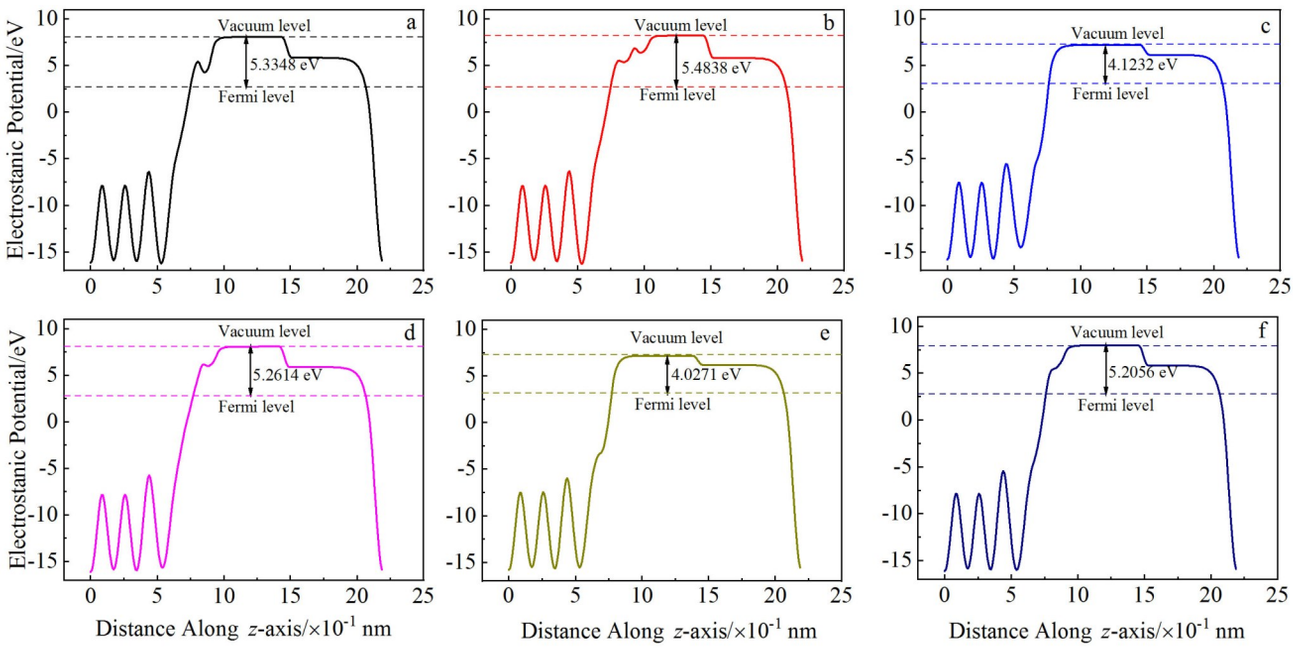

Fig.12 Electrostatic potential distributions along *z*-axis on *γ*-U(100)/4Mo slab surfaces with different configurations after O_2 molecule adsorption: (a) 4-T-Hor type, (b) 4-T-Ver type, (c) 4-H-Hor type, (d) 4-H-Ver type, (e) 4-B-Hor type, and (f) 4-B-Ver type

Table 4 Surface work function changes of *γ*-U(100)/Mo surfaces before and after O_2 molecule adsorption (eV)

Configuration	Vacuum level, E_{vacuum}	Fermi level, E_{Fermi}	Work function, Φ	Work function difference, $\Delta\Phi$
Free surface	7.2652	3.8115	3.4537	-
T-Hor	7.7632	3.8158	3.9474	0.4937
T-Ver	8.6057	3.5402	5.0655	1.6118
H-Hor	7.6196	3.8690	3.7506	0.2969
H-Ver	7.3408	4.0309	3.3099	−0.1438
B-Hor	7.4846	3.7256	3.7590	0.3053
B-Ver	8.3307	3.5955	4.7352	1.2815

Table 5 Surface work function changes of *γ*-U(100)/4Mo surfaces before and after O_2 molecule adsorption (eV)

Configuration	Vacuum level, E_{vacuum}	Fermi level, E_{Fermi}	Work function, Φ	Work function difference, $\Delta\Phi$
Free surface	7.0696	2.9724	4.0972	-
4-T-Hor	8.0603	2.7255	5.3348	1.2376
4-T-Ver	8.2201	2.7363	5.4838	1.3866
4-H-Hor	7.2077	3.0845	4.1232	0.0260
4-H-Ver	8.0723	2.8109	5.2614	1.1642
4-B-Hor	7.1855	3.1584	4.0271	−0.0701
4-B-Ver	7.9738	2.7682	5.2056	1.1084

The work functions are 3.4537 and 4.0972 eV for *γ*-U(100)/Mo and *γ*-U(100)/4Mo slabs before O_2 molecule adsorption, respectively. The work functions of all configurations for *γ*-U(100)/Mo surface increase after O_2 adsorption, except that of H-Ver configuration. As for the *γ*-U(100)/4Mo slab, the work functions all increase after O_2 adsorption, except that of 4-B-Hor configuration. After the stable adsorption of O_2 molecule, the electrons of U and Mo atoms on the surface transfer to O atoms, resulting in the negative charge of O atoms and the positive charge of U and Mo atoms. The surface dipole moment forms from the O atom to the adsorption surface, inducing the increase in surface work function. The work function increases less under the most stable configuration: the increment under H-Hor and 4-H-Hor configurations is 0.2969 and 0.0260 eV, respectively. After O_2 molecule adsorption, the O atoms are closer to the surface, and the charge transfer induces a minor dipole moment, which leads to a small change in the work function.

3 Conclusions

1) The O_2 adsorption on γ-U(100)/Mo and γ-U(100)/4Mo surfaces is chemical adsorption, i. e., O atoms form a stable chemical bond with U and Mo atoms on the surface.

2) The O_2 adsorption energy under the hollow-horizontal (H-Hor) and 4-hollow-horizontal (4-H-Hor) configurations is the lowest of −12.152 and −8.661 eV for the γ-U(100)/Mo and γ-U(100)/4Mo slabs, respectively. This also infers that H-Hor and 4-H-Hor configurations are the most stable adsorption structures for the γ-U(100)/Mo and γ-U(100)/4Mo slabs, respectively.

3) The work function increases after O_2 adsorption, and the increment under H-Hor and 4-H-Hor configurations is 0.2969 and 0.0260 eV, respectively, less than that under other configurations.

4) The charge transfers from U and Mo atoms to O atoms after O_2 molecule adsorption, resulting in the positively charged U and Mo atoms and negatively charged O atoms. The Bader charge number of O_2 molecule after dissociated adsorption (1.9326–2.3671 e) is significantly more than that after undissociated adsorption (0.5685–1.1961 e).

5) The bonding mode between O and U/Mo atoms is dominated by ionic bonding, and the reaction mechanism is the weak hybridization of O 2s orbital with U 6p orbital coupled with the strong hybridization of O 2p orbital with U 6d, Mo 5s, Mo 4p, and Mo 4d orbitals, which produces new chemical bonds. After O_2 molecule adsorption, the $2\pi^*$ orbital energy of O_2 molecule decreases, and the $2\pi^*$ orbital hybridizes with the 1π and 5σ orbitals.

References

1 Burke J J. *Physical Metallurgy of Uranium Alloys*[M]. Ohio: Metals and Ceramics Information Center, 1976

2 Gung G. *Critical Metals Handbook*[M]. Hoboken: John Wiley & Sons, 2014

3 Fairman H E, Kelly A. *Metallography and Microstructures of Uranium and Its Alloys*[M]. Russell: ASM International, 2004

4 Söderlind P, Eriksson O, Johansson B *et al*. *Nature*[J], 1995, 374(6522): 525

5 Li Gan, Luo Wenhua, Yin Chen. *Rare Metal Materials and Engineering*[J], 2011, 40(12): 2125 (in Chinese)

6 Haschke J M. *Journal of Alloys and Compounds*[J], 1998, 278(1–2): 149

7 Huang S S, Zeng X L, Zhao F Q *et al. Journal of Molecular Modeling*[J], 2016, 22: 88

8 Asada K, Ono K, Yamaguchi K *et al. Journal of Alloys and Compounds*[J], 1995, 231(1–2): 780

9 Shen Z Y, Kong Y, Du Y *et al. Calphad*[J], 2021, 72: 102 241

10 Bajaj S, Landa A, Söderlind P *et al. Journal of Nuclear Materials*[J], 2011, 419(1–3): 177

11 Tkach I, Kim-Ngan N H, Warren A *et al. Physica C: Superconductivity*[J], 2014, 498: 14

12 Kim-Ngan N H, Tkach I, Mašková S *et al. Journal of Alloys and Compounds*[J], 2013, 580: 223

13 Harris J, Andersson S. *Physical Review Letters*[J], 1985, 55(15): 1583

14 Chattaraj D, Parida S C, Majumder C. *Physica B: Condensed Matter*[J], 2011, 406(22): 4317

15 Huda M N, Ray A K. *International Journal of Quantum Chemistry*[J], 2005, 102(1): 98

16 Liu Zhixiao, Deng Huiqiu, Hu Wangyu. *The Chinese Journal of Nonferrous Metals*[J], 2013, 23(4): 1160 (in Chinese)

17 Liu G D, Liu Z X, Ao B Y *et al. Computational Materials Science*[J], 2018, 144: 85

18 Tian X F, Wang Y, Li L S *et al. Computational Materials Science*[J], 2020, 179(13): 101 963

19 Xiang S K, Huang H C, Hsiung L M. *Journal of Nuclear Materials*[J], 2008, 375(1): 113

20 Kresse G, Furthmüller J. *Computational Materials Science*[J], 1996, 6(1): 15

21 Kresse G, Hafner J. *Phys Rev B: Condens Matter*[J], 1993, 48(17): 13 115

22 Hohenberg P, Kohn W. *Physical Review*[J], 1964, 136(3): B864

23 Kohn W, Sham L J. *Physical Review*[J], 1965, 137(6A): 1697

24 Kresse G, Joubert D. *Physical Review B*[J], 1999, 59(3): 1758

25 Perdew J P, Chevary J A, Vosko S H *et al. Physical Review B*[J], 1992, 46(11): 6671

26 Perdew J P, Burke K, Ernzerhof M. *Physical Review Letters*[J], 1998, 77(18): 3865

27 Monkhorst H J, Pack J D. *Physical Review B*[J], 1976, 13(12): 5188

28 Payne M C, Teter M P, Allan D C *et al. Reviews of Modern Physics*[J], 1992, 64(4): 1045

29 Xiang S K, Huang H C, Hsiung L M. *Journal of Nuclear Materials*[J], 2008, 375(1) : 113

30 Chiotti P, Klepfer H H, Gill K J. *JOM*[J], 1957, 9: 51

31 Lide D R. *CRC Handbook of Chemistry and Physics*[M]. Boca Raton: CRC Press, 2004, 85: 423

32 Shi P, Yang Y, Ao B Y *et al. Journal of Physical Chemistry C*[J], 2014, 118(46): 26 634

33 Neugebauer J, Scheffler M. *Physical Review B*[J], 1992, 46(24): 16 067

34 Barrett S A, Jacobson A J, Tofield B C *et al. Acta Crystallographica Section B*[J], 1982, 38(11): 2775

35 Brandt B G. *Chemical Communications*[M]. Stockholm: University of Stockholm, 1971

36 Henkelman G, Arnaldsson A, Jónsson H. *Computational Materials Science*[J], 2006, 36(3): 354

37 *Electronegativity of Chemical Elements*[EB/OL]. https://material-properties.org/electronegativity-of-chemical-elements/

氧气在铀钼体系表面吸附和解离行为的第一性原理研究

李俊炜[1,2]，贾维敏[2]，吕沙沙[3]，王金涛[2]，李正操[1]

(1. 清华大学 材料学院，北京 100084)

(2. 西安高科技研究所，陕西 西安 710025)

(3. 北京师范大学 核科学与技术学院，北京 100875)

摘　要：基于第一性原理探究了氧气分子在铀钼表面的吸附解离行为。在五层γ-U(100)表面构型的基础上，用单个钼原子置换表层的1个高对称点的铀原子，并用4个钼原子置换表层铀原子后，分别建立了γ-U(100)/Mo和γ-U(100)/4Mo模型，计算得到了不同吸附构型下的结构参数、吸附能、Bader电荷、电子结构和表面功函数。结果表明，氧分子在γ-U(100)/Mo和γ-U(100)/4Mo表面为化学吸附，且最稳定的吸附位点为空位平行吸附，吸附能分别为−12.552和−8.661 eV。氧分子在铀钼表面的吸附分为解离吸附和未解离吸附，两者共同组成稳定的吸附行为，同时，解离吸附比未解离吸附更为稳定。Bader电荷结果表明，氧气在吸附过程中，主要与吸附表面最上两层的原子发生电荷转移。电子结构研究表明，O 2s和U 6p轨道发生轻微杂化，O 2p与U 6d、Mo 5s、Mo 4p、Mo 4d轨道发生较强的重叠杂化。本研究为氧分子在铀钼合金表面的吸附提供了机理阐述，并进一步为氧气在铀钼合金表面的腐蚀机理研究提供理论基础。

关键词：铀钼合金；解离吸附；轨道杂化；第一性原理

作者简介：李俊炜，男，1997年生，博士生，清华大学材料学院，北京 100084，E-mail：lijunwei21@mails.tsinghua.edu.cn